CrossMark

Synthesis and catalytic hydrogenation activity of Pd and bimetallic Au–Pd nanoparticles supported on high-porosity carbon materials

Oleg V. Belousov[1] · Valery E. Tarabanko[1] · Roman V. Borisov[1] ·
Irina L. Simakova[2] · Anatoly M. Zhyzhaev[1] · Nikolay Tarabanko[1] ·
Victoria G. Isakova[3] · Vladimir V. Parfenov[1] · Ilya V. Ponomarenko[1]

Abstract The processes of palladium deposition on various high-porosity carbon matrices (Sibunit, CMK-3) have been studied. Mesostructured carbon material CMK-3 was synthesized using a silicate template of SBA-15 type. Pd nanoparticles were loaded onto carbon matrices by metalorganic chemical vapour deposition (MOCVD) method using palladium(II) acetylacetonate precursor. Bimetal Au–Pd systems were synthesized by autoclave reduction of gold(III) chloride complexes on Pd-containing carbon matrices. Structure of the obtained composite particles was studied by electron microscopy and X-ray diffraction. The average diameter of Pd particles on Sibunit is about 10, and 5–6 nm on CMK-3. The catalytic activity of the synthesized materials was studied in the reaction of furfural diethyl acetal (FDEA) hydrogenation, using gas–liquid chromatographic analysis. There is significant difference in catalytic activity of MOCVD-Pd/C compared to conventional impregnated Pd/C systems: the hydrogenation rate is 3–6 times higher with MOCVD-derived catalysts. Introducing Au into a MOCVD-Pd/C catalyst increases the hydrogenation rate threefold. Considerable difference in the composition of hydrogenation products was observed between these differently prepared catalysts.

Keywords MOCVD · Hydrothermal synthesis · Palladium nanoparticles · Mesostructured carbon · Bimetallic Pd–Au catalyst · Furfural diethyl acetal · Hydrogenation

✉ Roman V. Borisov
  roma_boris@list.ru

1 Institute of Chemistry and Chemical Technology of the Siberian Branch of the Russian Academy of Sciences - A Separate Division of FSC KSC SB RAS, 50/24, Akademgorodok, Krasnoyarsk, Russia 660036

2 Boreskov Institute of Catalysis, 5, Lavrentieva, Novosibirsk, Russia 630090

3 Kirensky Institute of Physics of the Siberian Branch of the Russian Academy of Sciences - A Separate Division of FSC KSC SB RAS, 50/38, Akademgorodok, Krasnoyarsk, Russia 660036

Introduction

Finely dispersed noble metals supported on highly porous carbon matrices are high-performance catalysts in the main processes of petrochemistry and hydrogen energy technology. They can also be used as the recognition element in electrochemical sensors toward hydrogen and carbon monoxide [1–4]. Recently, many papers are being devoted to noble metal introduction into carbon matrices, including such porous materials as Sibunit [5–7] and CMK-3 [8, 9]. Pd-containing catalysts are widely used in hydrogenation processes [10–12].

There is active ongoing research into new methods of improving the efficiency of this catalyst type. The last decade saw a significant increase in the number of articles devoted to synthesis and properties of composite bimetallic systems—in particular, Au–Pd nanoparticles based on carbon supports [13]. Bimetallic Au–Pd nanoparticles introduced into carbon matrices have higher catalytic performance in comparison with their monometallic counterparts [14, 15]. Another promising field of study is the use of mesoporous and/or mesostructured carbon materials like CMK-3. Their obvious advantage is highly ordered porosity [16]. The combination of XRD and gas absorption methods allows researchers [16] to deduce the structure of these materials with the detail level that is impossible for most other carbon matrices. Moreover, template synthesis of CMK-3 unlocks the opportunity of fine-tuning the carbon material porous structure by varying the porous structure of silica templates (like SBA-15). Therefore, the CMK-3 carbon support is a very suitable model object of study.

Carbon-supported Pd nanoparticles can be obtained via different methods. Several examples are impregnation with Pd-containing solution followed by reduction to metallic state [17], metal precipitation from gaseous volatile organometallic substances [18], thermolysis of ammonia complexes [19].

Chemical vapor deposition method allows synthesizing nanoparticles on different substrates including porous materials and powders. It is based on vapor-phase chemical decomposition of volatile metal precursor compounds. In recent years, intense development of different modifications to vapor deposition methods for catalytic applications took place, for example, atomic layer deposition (ALD) [20].

As for noble bimetal nanoparticles, the general approach of synthesis is sequential or simultaneous reduction from solutions of metal complexes using various reductants and stabilizers [21].

The synthesis of bimetallic Au–Pd solid solution by means of reductive thermolysis is quite interesting [22]. This method involves the decomposition of double complex salts of metals when heated in air or inert gas atmosphere which produces nanosized phases of solid solutions. Another effective method of obtaining bimetallic nanoparticles is contact reduction of noble metals from solution by nanocrystalline powders [23–25]. Such reactions constitute a promising approach for formation of purpose-designed materials, for example coatings or polymetallic powders with varying dispersity, chemical and phase composition.

Among the hydrogenation processes, catalytic conversion of furfural attracts strong and continuous interest due to its bifunctionality (carbonyl group and furan

ring) and its ability to serve as a base for renewable plant feedstock derived engine fuels [26]. Traditional and contemporary carbon-supported copper catalysts of furfural hydrogenation in vapor phase [27] operate at temperatures above 200 °C under hydrogen pressures 70–100 bar [28]. Nickel catalysts on carbon operate at modest temperatures (70 °C and above), but require high hydrogen pressure (4 MPa), and yield primarily tetrahydrofurfuryl alcohol [29]. Nickel-boron alloys [30] catalyze hydrogenation of furfural at 70 °C and hydrogen pressure 1 MPa. It is believed that the Lewis acid sites of the Ni–B catalyst activate the carbonyl group of furfural for hydrogenation [30]. According to the review [30], copper-containing catalysts are the most selective ones for hydrogenation of furfural to furfuryl alcohol.

Catalysis by bimetallic systems attracts considerable attention, as different metals often exhibit synergistic effects upon the rate as well as the selectivity of furfural hydrogenation. Adding palladium to a nickel catalyst increases the selectivity towards tetrahydrofurfuryl alcohol, while adding rhenium to a platinum catalyst allows attaining 95% selectivity in furfuryl alcohol with full conversion of furfural [31].

Palladium catalysts on carbon can hydrogenate furfural in liquid phase (100 °C, 3 MPa of hydrogen, 5 h) leading primarily to tetrahydrofurfuryl alcohol; platinum catalysts yield furfuryl alcohol [28]. Addition of iron, cobalt, nickel, and manganese to either palladium or platinum catalyst leads to higher furfural conversion. When added to the platinum catalyst, these additives lead to higher selectivity in furfuryl alcohol, but with the palladium catalyst they result in (less distinct) decrease thereof. The higher conversion and/or selectivity imparted by the promoters may be viewed from two angles: one is the catalytic active sites interacting with the promoters, the other is contribution of electrons from the promoters to Pt and Pd due to alloy formation [28].

Addition of Sn to Ru/C catalysts results in both higher rate and selectivity in hydrogenation of furfural into furfuryl alcohol, and the dependency of these effects versus tin concentration is extremal in nature [32]. This result could be attributed to the fact that tin reduces the adsorption of hydrogen on the ruthenium surface, thus increasing the availability of the sites for furfural hydrogenation [32]. This explanation has been proposed, among others, by Zhang et al., who suggested that the reactivity of platinum catalysts in furfural hydrogenation could be improved by lowering the adsorption of H_2 via the addition of Ni and/or Cu [33].

Polar solvents, alcohols foremost, are preferential for liquid-phase furfural hydrogenation [28, 31, 34–37]; but much like the processes mentioned above, these ones require high hydrogen pressures (around 10 MPa). An exception is hydrogenation of 5-hydroxymethylfurfural into 2,5-dimethylfuran with a Pd–Au/C catalyst in tetrahydrofuran [26]. It should be mentioned that the presence of alcohols causes considerable acetalization of furfural [28, 34, 35], and the resulting acetals are hydrogenated into alkyl furfuryl ethers [26–35, 38] re promising biofuels [34–36].

The hydrogenation of furfural acetals is practically unexplored, and it is indubitably interesting in the context of biofuels production because the unstable carbonyl group is transformed into a more stable etheric group with

minimal consumption of hydrogen. For these reasons, ethyl furfuryl ether is considered a very promising high-octane additive to gasoline [34, 36]. The most effective system that can be used for this purpose appears to be a carbon-supported palladium-gold catalyst with tetrahydrofuran as the solvent, similarly to [26].

This paper presents the first results in hydrogenation of furfural diethyl acetal in tetrahydrofuran mediated by herein pioneered novel carbon-supported palladium and gold–palladium catalysts.

Experimental

Materials and methods

All reagents used in this work were of analytical grade qualification. Hydrochloric acid was purified by sub-boiling using a DuoPur apparatus (Milestone Inc). Solutions were prepared using deionized water (Direct-Q3 purification system, Millipore). Synthesis of CMK-3 was performed according to a previously published procedure [39]: First, silica matrix SBA-15 is twice impregnated with sucrose solution, then high temperature carbonization in inert atmosphere proceeds. Afterwards, the silica matrix was dissolved in alkali.

Palladium diacetylacetonate (Pd(acac)$_2$) was synthesized according to a technique described elsewhere [40]. Furfural diethyl acetal was obtained by reaction of furfural with triethyl orthoformate [41]. Ethyl furfuryl ether was synthesized via a known procedure [42].

Metal concentration in solution was determined by AAS (AAnalist 400, PerkinElmer) and MS-ICP (Agilent7500a). The weight of solid residue was measured by analytical balance (Mettler Toledo XP 205 DR). XRD was performed on powder diffractometer PANalytical X'Pert PRO MPD with Cu K$_{\alpha 1}$ radiation source and carbon monochromator, 2θ angle range 30–90°. Microstructural parameters were calculated by Rietveld profile refinement method [43].

The nitrogen adsorption isotherms and pore size distributions were obtained with an ASAP 2420 (Micromeritics Inc.) at nitrogen boiling point (77 K). Samples were preliminarily outgassed at 343 K in vacuum (1.2 Pa). Nitrogen adsorption was registered in the P/P$_0$ range 0–0.99 in fixed volume dosing mode. Textural characteristics were calculated by single point, BET, t-plot and BJH methods.

Chemical composition of solids was determined by full dissolution of powder samples in aqua regia, and subsequent AAS analysis of metal concentrations.

For SEM imaging, a Hitachi S5500 instrument with Thermo Scientific Noran Spectral System EDS was used.

Impregnation of palladium on carbon materials

A solid mixture of a mesoporous carbon material ($\sim$ 200 mg) and Pd(acac)$_2$ ($\sim$ 25 mg) was finely ground in a mortar, loaded into a flat-bottomed quartz crucible, and heated in air to autoignition (180–200 °C). The process was continued for 10-15 min in flameless mode without significant temperature increase. Weighing

the combustion products reveals that the mass loss of the samples is equal to the ligand mass in the initial Pd(acac)$_2$. For reference experiments, traditional 6% Pd/C catalyst was obtained by impregnation of Subunit mesoporous carbon (S = 355 m^2/g) with palladium chloride solution, and subsequent metal reduction in hydrogen flow with heating to 250 °C (1.5 °C/min) [34–36].

Synthesis of Au–Pd/C composites

Synthesis of bimetallic Au–Pd particles on the herein above described Pd/C materials was accomplished according to the original technique [23] via autoclave reduction of HAuCl$_4$ solutions in hydrochloric acid according to Eq. 1:

$$2HAuCl_4 + 3Pd + 4HCl \rightarrow 2Au + 3H_2PdCl_4 \tag{1}$$
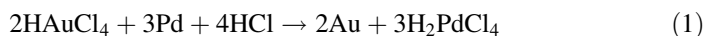
This processes was executed in a quartz reactor of 50 cm^3 volume at 130 °C under argon atmosphere for 120 min. Pd:Au molar ratio was 10:1. Temperature uniformity was attained by continuous vertical agitation [23].

Catalyst activity tests

The experiments with liquid phase hydrogenation of furfural diethyl acetal were carried out in tetrahydrofuran medium in a glass reactor with reflux condenser at 60 °C. THF was chosen as the solvent because the initial acetal and the reaction products are well soluble in THF, THF is not converted under the reaction conditions, and its retention time in GC analysis is distinct from that of the other solution components. Moreover, THF is known to have been used used for hydrogenation of 5-HMF at atmospheric pressure [26]. A catalyst sample (0.2 g) was loaded into the reactor and conditioned by hydrogen flow at 200 °C for 60 min. Reaction mixture of FDEA (0.24 ml) and the solvent (20 ml) was used. Hydrogen from a cylinder was passed through a pipe filled with Ni–Cr catalyst (NIAP-12-05, Novomoskovsk, Russia, reduced with hydrogen flow 120 cm^3/min at 450 °C for 9 h) to remove oxygen, and through a pipe filled with desiccant (ZSM zeolite) to remove water before being fed into the reactor. The reaction mixture was regularly sampled and analyzed. The products were identified by GC–MS, Agilent 5973N EI/PCI (column 30 m × 0.25 mm HP-5ms). Quantitative analysis of the reaction products was done with Chromos GC-1000 chromatograph equipped with a flame ionization detector using BP20 capillary column (60 m/0.25 mm/0.25 μm) at 323–473 K and a heating rate of 10 K/min. The temperature of the detector was the same as for the evaporator (523 K), the carrier gas was hydrogen with the flow rate 20 cm^3/min. Chromatograms were processed using the Gepard software. Calibration was performed against individual synthesized substances.

The data on hydrogenation kinetics were processed as an approximation of a first-order reaction with respect to the substrate concentration. The calculations were performed with the Origin 7.0 SR0 software; standard deviation values of the approximation are taken as the error of rate constants determination.

Results and discussion

Carbon matrices

The textural parameters of the carbon materials used in this study are presented in Table 1.

The two carbon materials have similar texture parameters but significantly different layout of their pore space. In Sibunit, pores smaller than 2.7 nm constitute approximately a half of its specific pore volume, while pores smaller than 1.6 nm account for about a half of its specific surface area. The pore size distribution has no clearly defined maxima (Fig. 1). The average pore diameter (cylindrical pore approximation) is about 11 nm.

CMK-3 has significantly more accessible surface. Pores smaller than 5.7 nm make up about half of its specific pore volume, and pores smaller than 2.9 nm give about half of its specific area. The pore size distribution has one clearly defined maximum near 3.3 nm (Fig. 1) and conventional average pore diameter (cylindrical pore approximation) is about 7.2 nm. The main difference between these two materials is their surface curvature. CMK-3 has practically no surface with negative curvature. It is essentially constructed out of carbon rods that are held in a regular arrangement by cylindrical bridges [44]. The distance between these rods is defined by the wall thickness of the silica precursor SBA-15 and equals to 2.5–3.5 nm. The volume of micropores in CMK-3 is less than 6% of the entire pore volume. Therefore, the material's inner surface is easily accessible since in such structures there are no mass transfer bottlenecks at pore inlets. Moreover, every pore is connected to every neighboring one, so the entire pore volume of a carbon matrix particle is dimensionally contiguous throughout the particle. With Sibunit, the porous structure is quite irregular, and every pore is different. Their surface is generally concave. Electron microscope images of CMK-3 and Sibunit particles are presented in Fig. 2.

Deposition of Pd on carbon substrates

We used simple MOCVD technique with $Pd(acac)_2$ and oxygen as the reactants for obtaining palladium nanoparticles on carbon support. This technique was earlier used for synthesis of Pt and Pd nanoparticles on detonation nanodiamond (DND) powders [45]. The heating of $Pd(acac)_2$/CMK-3 (or Sibubit) mixtures leads to its

Table 1 Texture characteristics of the carbon materials

Matrix	Specific area (m^2/g)	Specific pore volume (sm^3/g)	Average pore diameter (4 V/S) (nm)	Maximum of pore size distribution (nm)
Sibunit	500	1.34	10.7	–
CMK-3	750	1.35	7.2	3.3

Fig. 1 Pore size distribution in the carbon materials
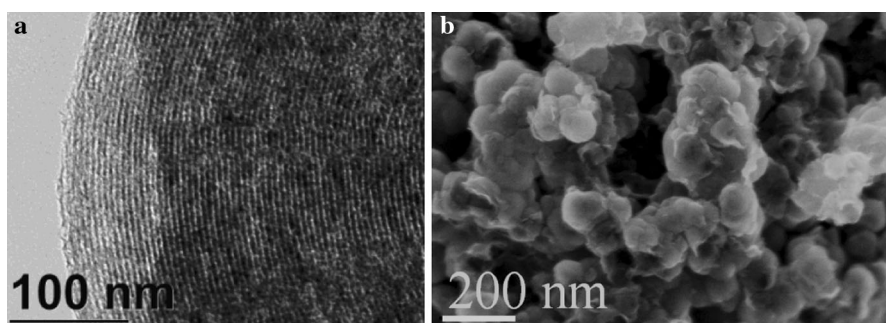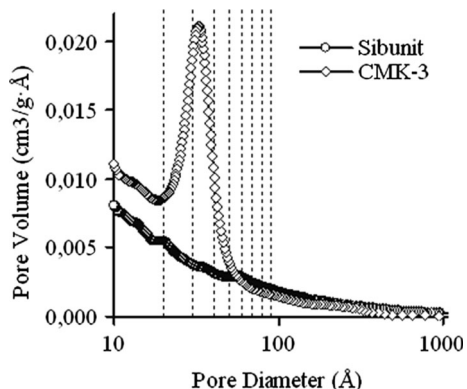

Fig. 2 **a** TEM image of carbon material CMK-3, **b** SEM image of carbon material Sibunit

autoignition at 180–200 °C (that corresponds to Pd(acac)$_2$ sublimation temperature [46]) and subsequent flameless combustion (smoldering) at 200–250 °C. In this work, combustion time was short (15 min) with air access limitation in order to prevent the carbon support oxidation.

The mechanism of the Pd/C composite synthesis is probably catalytic oxidation like earlier observed for an ALD processes involving metal acetylacetonate oxidation [47]. However, in our case, supplying both reactants (Pd(acac)$_2$ and O$_2$) to a carbon substrate was performed simultaneously, unlike the prior art that used pulse feeding (first metal precursor, then oxygen). The ligand combustion and Pd particles formation occurs after Pd(acac)$_2$ chemisorption on the substrate surface.

The metal crystallite size depends on the amount of the deposited metal, with higher dispersion corresponding to lower metal concentration [48]. For example, catalytic-combustion-derived Pt/DND and Pd/DND composites exhibit average metal crystallite sizes 25 and 10 nm for 10 and 5 wt% metal loading respectively, as calculated by the Scherrer method [45]. In the present work, we obtained about 6 wt% palladium applied on porous Sibunit or CMK-3. Overview SEM images of these samples are presented in Fig. 3. According to these data, the metal distribution on the substrate surface is quite uniform. The average diameter of Pd particles is about 10 nm on Sibunit and 5–6 nm on CMK-3. The SEM images reveal no larger
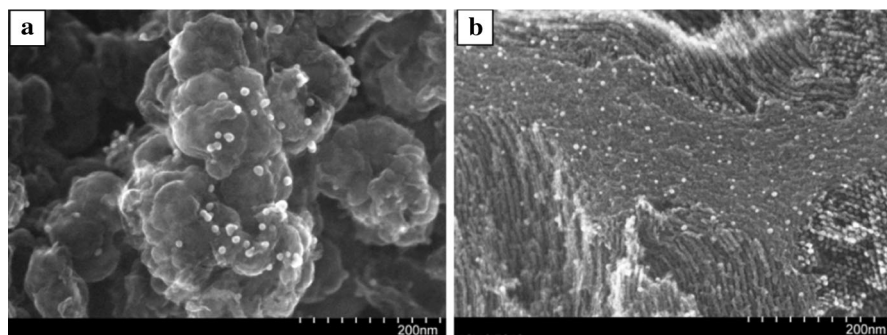
Fig. 3 SEM images of Pd/Sibunit **a** and Pd/CMK-3 **b** MOCVD-derived composites (6 wt% Pd)

particles. In comparison, impregnation-derived catalyst (6 wt% Pd on Sibunit) exhibits metal particle size of about 3.2 nm [34].

XRD pattern of the Pd/Sibunit MOCVD-derived sample (Fig. 4) shows reflexes characteristic for metallic palladium. The Pd crystallite size calculated using XRD line width agrees with the particle size obtained by SEM.

Bimetallic particles on carbon

In our previous work [23], it was shown that under hydrothermal conditions it is possible to produce bimetal nanoparticles of various compositions. Palladium can reduce gold(III) from hydrochloric solutions according to Eq. 1. This interaction creates Pd–Au bimetallic particles consisting of a palladium core surrounded by a gold–palladium solid solution shell. Composition of the solid solution can be controlled by changing the molar ratio Pd/Au, process duration, and temperature [23]. It is necessary to account for the possibility of nanosized Pd partial dissolution in hydrochloric acid due to oxidation by chemisorbed oxygen [49]:
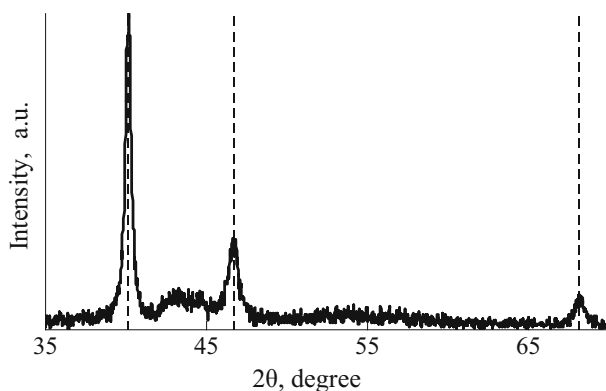
Fig. 4 Fragment of XRD pattern of Pd/Sibunit composite (6 wt% Pd)

$$2Pd + O_2 + 8HCl \rightarrow 2H_2PdCl_4 + 2H_2O. \tag{2}$$
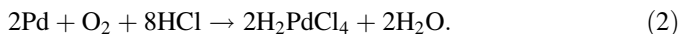
In order to exclude the interaction of palladium with dissolved or ambient oxygen, the process was conducted under argon atmosphere [23].

In the present work, the reaction between the Pd/Sibunit composite and $HAuCl_4$ solution (C_{Au} = 0.5 mmol/l, initial molar ratio Pd:Au is 10:1) at 130 °C for 120 min results in quantitative gold reduction. Thereby, up to 30% of the palladium metal is dissolved. Material balance considerations lead to the following composition of the Pd–Au/Sibunit system—3 wt% Pd and 1 wt% Au. This composition is in good agreement with the SEM–EDS analysis results: the mass ratio Pd:Au in different sample spots varies from 3:2 to 4:1. Size of the Pd–Au bimetal particles is 30–80 nm (Fig. 5), the particles are nearly spherical in shape. Gold and palladium are quite uniformly distributed on the Sibunit surface; the fact that gold does not preferentially concentrate in any particular region of the surface suggests that the reduction of gold(III) is only caused by the cementation reaction (1) [25].

Besides the reflexes from the carbon support, XRD analysis detects the signals from palladium metal and a gold-rich solid solution $Au_{0.9}Pd_{0.1}$ (Fig. 6). The diffractograms exhibit wide peaks that may be caused by irregularities in the chemical composition and high dispersity of the metal phases.

Catalytic activity in hydrogenation of furfural diethyl acetal

The obtained metal/carbon composite systems were tested as catalysts in the hydrogenation of furfural diethyl acetal. The reaction was conducted in the absence of mass transfer limitations (gas–liquid, liquid–solid and internal diffusion) under reaction conditions comparable to some literature data where the absence of mass transfer limitations was verified [50, 51].

Fig. 7 presents kinetic curves of FDEA consumption during hydrogenation mediated by the four synthesized catalysts. Table 2 presents the values of rate constants for first-order kinetic equation with respect to formation of the principal products of FDEA hydrogenation: tetrahydrofurfural diethyl acetal and furfural. The Au–Pd catalyst is the most active one; its precursor (MOCVD Pd/Sibunit) is three times less active. Even lower activity is exhibited by the impregnated catalyst on

Fig. 5 SEM-image of Au Pd particles on Sibunit
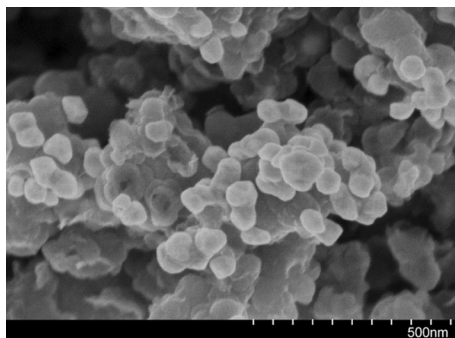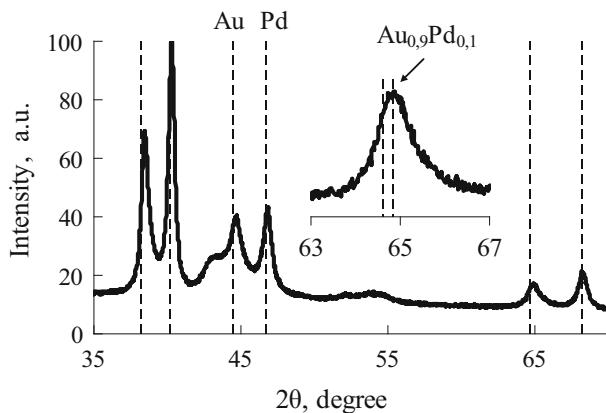
Fig. 6 Fragment of XRD pattern of the Au–Pd/Sibunit composite
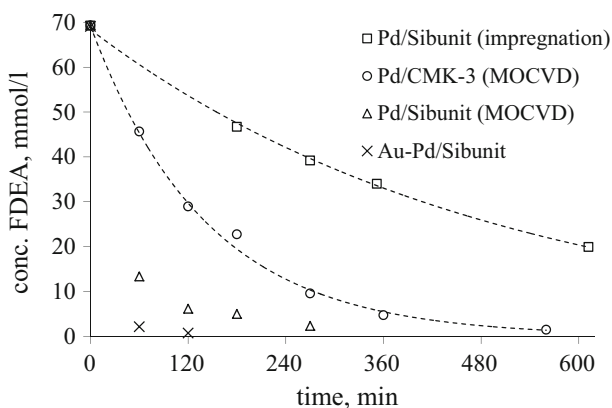
Fig. 7 The conversion of the furfural diethyl acetal in the hydrogenation process in tetrahydrofuran solution on different catalysts (FDEA in 0.071 M tetrahydrofuran, catalyst loading 0.5%, 60 °C, atmospheric pressure, hydrogen flow)

Sibunit. Interestingly, depositing palladium onto Sibunit by MOCVD produces more active catalyst than impregnation despite the fact that the former contains larger palladium particles.

The mass balance in carbon accounted as the yield sum of furan- and tetrahydrofuran-type products is not high, attaining 45–85 mol%. This is probably related to the propensity for condensation reactions that is typical for furfural derivatives [52].

The studied process can take different chemical pathways, but the principal routes are the furan ring transformation into the tetrahydrofuran one (3), and hydrogenolysis of the acetal group into ether (5) [34, 35] or into furfural (Scheme 1, Eq. 4):

Formation of furfural over the MOCVD Au–Pd/Sibunit and Pd/Sibunit can proceed via hydrogenolysis of the ether bond $O–C_2H_5$ which leads to the

Table 2 Rate constants and carbon balance of the furfural diethyl acetal (FDEA) hydrogenation

Catalyst	Rate constant of hydrogenation (min^{-1})	Rate constants of the product formation (min^{-1})		Carbon balance at t = min
		THFDEA	Furfural	
	$\times\ 10^3$			
Pd/Sibunit (impregnation)	2.0 ± 0.4	2.8 ± 0.36	–	85
Au–Pd/Sibunit	38 ± 11	–	11 ± 1	45
Pd/Sibunit (MOCVD)	12 ± 2.4	–	19 ± 3	65
Pd/CMK-3 (MOCVD)	7.1 ± 0.24	5.9 ± 0.83	–	50
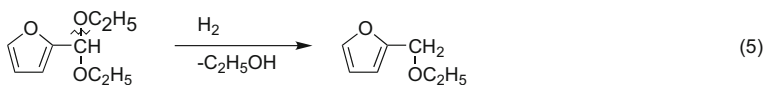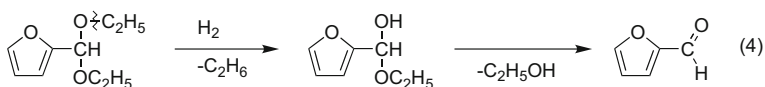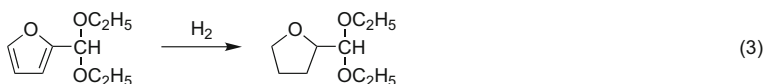
Scheme 1 Possible pathways of furfural diethyl acetal hydrogenation

hemicateal, and the latter spontaneously decomposes releasing ethanol (4) [53]. Hydrogenolysis of FDEA into ethyl furfuryl ether (up to 4 mol%, Eq. 5) and ethyl tetrahydrofurfuryl ether (up to 20 mol%) takes place in the second process cycle (i.e., with already used catalyst) over Pd/CMK-3 (MOCVD). Manifestation of this pathway may be related to formation of partially oxidized palladium species during handling of the catalyst between the process cycles in ambient air.

The sixfold difference in activity between the impregnated and the MOCVD palladium catalysts might be caused by lower stability of the former against metal agglomeration during the hydrogenation. Higher activity of the Au–Pd catalyst compared to the monometallic palladium can be explained by several hypotheses described above [28, 32, 33, 54, 55]. The most likely explanation of this phenomenon can be linked to lower hydrogen solubility in the Au–Pd solid solution compared to pure palladium [56, 57]. This leads to lower hydrogen adsorption on the metal surface, leaving more catalytic sites for adsorbing diethyl acetal of furfural [32].

Conclusion

The obtained results demonstrate (a) a new method for synthesis of catalysts based on low-temperature gas-phase oxidation of volatile palladium diacetylacetonate (MOCVD method); (b) palladium-gold bimetal catalyst synthesis via autoclave reduction of $HAuCl_4$ solutions with nanosized palladium particles; (c) the MOCVD catalysts are more active as compared to traditional impregnated one; (d) furfural diethyl acetal is shown to be hydrogenated into tetrahydrofurfural diethyl acetal and ethylfurfuryl ether.

References

1. Ferrando R, Jellinek J, Johnston RL (2008) Nanoalloys: from theory to applications of alloy clusters and nanoparticles. Chem Rev 108:845–910. https://doi.org/10.1021/cr040090g
2. Wu B, Kuang Y, Zhang X, Chen J (2011) Noble metal nanoparticles/carbon nanotubes nanohybrids: synthesis and applications. NanoToday 6(1):75–90. https://doi.org/10.1016/j.nantod.2010.12.008
3. Qin YH, Li Y, Lv RL, Wang TL, Wang WG, Wang CW (2014) Pd–Au/C catalysts with different alloying degrees for ethanol oxidation in alkaline media. Electrochim Acta 144:50–55. https://doi.org/10.1016/j.electacta.2014.08.078
4. Dimitratos N, Hammond C, Kiely CJ, Hutchings GJ (2014) Catalysis using colloidal-supported gold-based nanoparticles. Appl Petrochem 4(1):85–94. https://doi.org/10.1007/s13203-014-0059-9
5. Madsen AT, Rozmysłowicz B, Mäki-Arvela P, Simakova IL, Eränen K, Murzin DY, Fehrmann R (2013) Deactivation in continuous deoxygenation of C18-fatty feedstock over Pd/Sibunit. Top Catal 56(9–10):714–724. https://doi.org/10.1007/s11244-013-0030-5
6. Bonarowska M, Pielaszek J, Semikolenov VA, Karpiński Z (2002) Pd–Au/sibunit carbon catalysts: characterization and catalytic activity in hydrodechlorination of dichlorodifluoromethane (CFC-12). J Catal 209(2):528–538. https://doi.org/10.1006/jcat.2002.3650
7. Smirnova NS, Shlyapin DA, Leont'eva NN, Trenikhin MV, Shitova NB, Kochubey DI, Tsyrul'nikov PG (2015) Comparative EXAFS and TEM study of Pd/Sibunit and Pd–Ga/Sibunit catalysts for liquid-phase acetylene hydrogenation. Bull Russ Acad Sci 79(9):1186–1190. https://doi.org/10.3103/s106287381501030x
8. Hao Y, Hao GP, Guo DC, Guo CZ, Li WC, Li MR, Lu AH (2012) Au–Pd nanoparticles confined in tubular mesoporous carbon as highly selective and reusable benzyl alcohol oxidation catalysts. ChemCatChem 4(10):1595–1602. https://doi.org/10.1002/cctc.201200207
9. Wang Z, Chen W, Han Z, Zhu J, Lu N, Yang Y, Huang S (2014) Pd embedded in porous carbon (Pd@CMK-3) as an active catalyst for Suzuki reactions: accelerating mass transfer to enhance the reaction rate. NanoResearch 7(9):1254–1262. https://doi.org/10.1007/s12274-014-0488-x
10. Yarulin AE, Crespo-Quesada RM, Egorova EV, Kiwi-Minsker LL (2012) Structure sensitivity of selective acetylene hydrogenation over the catalysts with shape-controlled palladium nanoparticles. Kinet Catal 53(2):253–261. https://doi.org/10.1134/S0023158412020152
11. Chen A, Ostrom C (2015) Palladium-based nanomaterials: synthesis and electrochemical applications. Chem Rev 115(21):11999–12044. https://doi.org/10.1021/acs.chemrev.5b00324
12. Ukraintsev VB, Khokhryakov KA, Sobolev NZ (2010) Catalytic activity in hydrogenation processes of catalysts containing nanodimensional palladium on carbon support. Concentration effect of palladium and precursor. Russ J Gen Chem 80(4):866–867. https://doi.org/10.1134/S1070363210040304
13. Kunal P, Li H, Dewing BL, Zhang L, Jarvis K, Henkelman G, Humphrey SM (2016) Microwave-assisted synthesis of PdxAu(100 − x) alloy nanoparticles: a combined experimental and theoretical assessment of synthetic and compositional effects upon catalytic reactivity. ACS Catal 6(8):4882–4893. https://doi.org/10.1021/acscatal.6b01014
14. Zhou W, Lee JY (2007) Highly active core–shell Au@Pd catalyst for formic acid electrooxidation. Electrochem Commun 9(7):1725–1729. https://doi.org/10.1016/j.elecom.2007.03.016

15. Zhang S, Qing M, Zhang H, Tian Y (2009) Electrocatalytic oxidation of formic acid on functional MWCNTs supported nanostructured Pd–Au catalyst. Electrochem Commun 11(11):2249–2252. https://doi.org/10.1016/j.elecom.2009.10.001

16. Shinae J, Joo SH, Ryoo R, Kruk M, Jaroniec M, Liu Z, Ohsuna T, Terasaki O (2000) Synthesis of new, nanoporous carbon with hexagonally ordered mesostructure. J Am Chem Soc 122(43):10712–10713. https://doi.org/10.1021/ja002261e

17. Li H, Sun G, Jiang Q, Zhu M, Sun S, Xin Q (2007) Synthesis of highly dispersed Pd/C electrocatalyst with high activity for formic acid oxidation. Electrochem Commun 9(6):1410–1415. https://doi.org/10.1016/j.elecom.2007.01.032

18. Meille V (2006) Review on methods to deposit catalysts on structured surfaces. Appl Catal A 315:1–17. https://doi.org/10.1016/j.apcata.2006.08.031

19. Belousov OV, Sirotina AV, Belousova NV, Fesik EV, Borisov RV, Malchikov GD (2014) Formation of nanomaterials based on non-ferrous and noble metals in autoclaves. J Sib Fed Univ Eng Technol 7(2):138–145

20. O'Neill BJ, Jackson DHK, Lee J, Canlas C, Stair PC, Marshall CL, Elam JW, Kuech TF, Dumesic JA, Huber GW (2015) Catalyst design with atomic layer deposition. ACS Catal 5(3):1804–1825. https://doi.org/10.1021/cs501862h

21. Zaleska-Medynska A, Marchelek M, Diak M, Grabowska E (2016) Noble metal-based bimetallic nanoparticles: the effect of the structure on the optical, catalytic and photocatalytic properties. Adv Colloid Interface Sci 229:80–107. https://doi.org/10.1016/j.cis.2015.12.008

22. Plyusnin PE, Baidina IA, Shubin YV, Korenev SV (2007) Synthesis, crystal structure, and thermal properties of [Pd(NH$_3$)$_4$][AuCl4]$_2$. Russ J Inorg Chem 52(3):371–377. https://doi.org/10.1134/S0036023607030138

23. Belousov OV, Belousova NV, Sirotina AV, Solovyov LA, Zhyzhaev AM, Zharkov SM, Mikhlin YL (2011) Formation of bimetallic Au–Pd and Au–Pt nanoparticles under hydrothermal conditions and microwave irradiation. Langmuir 27(18):11697–11703. https://doi.org/10.1021/la202686x

24. Kovalenko NL, Belousov OV, Dorokhova LI, Zharkov SM (1995) A study of the increase in sized of particles of palladium and rhodium blacks and the mechanisms of the solid solution formations in cementing reactions. Russ J Inorg Chem 40(4):657–661

25. Borisov RV, Belousov OV, Zhizhaev AM, Dorokhova LI (2015) Autoclave synthesis Pd–Au and Pd–Pt nanoparticles on carbon substrates. J Sib Fed Univ Chem 8:377–385. https://doi.org/10.17516/1998-2836-2015-8-3-377-385

26. Nishimura S, Ikeda N, Ebitani K (2014) Selective hydrogenation of biomass-derived 5-hydroxymethylfurfural (HMF) to 2, 5-dimethylfuran (DMF) under atmospheric hydrogen pressure over carbon supported PdAu bimetallic catalyst. Catal Today 232:89–98. https://doi.org/10.1016/j.cattod.2013.10.012

27. Rao RS, Baker RTK, Vannice MA (1999) Furfural hydrogenation over carbon-supported copper. Catal Lett 60(1–2):51–57

28. Liu L, Lou H, Chen M (2018) Selective hydrogenation of furfural over Pt based and Pd based bimetallic catalysts supported on modified multiwalled carbon nanotubes (MWNT). Appl Catal A 550:1–10. https://doi.org/10.1016/j.apcata.2017.10.003

29. Gong W, Chen C, Zhang H, Zhang Y, Zhang Y, Wang G, Zhao H (2017) Highly selective liquid-phase hydrogenation of furfural over N-doped carbon supported metallic nickel catalyst under mild conditions. Mol Catal 429:51–59. https://doi.org/10.1016/j.molcata.2016.12.004

30. Li H, Zhang S, Luo H (2004) A Ce-promoted Ni–B amorphous alloy catalyst (Ni–Ce–B) for liquid-phase furfural hydrogenation to furfural alcohol. Mater Lett 58(22–23):2741–2746. https://doi.org/10.1016/j.matlet.2004.04.003

31. Chen B, Li F, Huang Z, Yuan G (2015) Tuning catalytic selectivity of liquid-phase hydrogenation of furfural via synergistic effects of supported bimetallic catalysts. Appl Catal A 500:23–29. https://doi.org/10.1016/j.apcata.2015.05.006

32. Musci JJ, Merlo AB, Casella ML (2017) Aqueous phase hydrogenation of furfural using carbon-supported Ru and RuSn catalysts. Catal Today 296:43–50. https://doi.org/10.1016/j.cattod.2017.04.063

33. Zhang C, Lai Q, Holles JH (2017) Bimetallic overlayer catalysts with high selectivity and reactivity for furfural hydrogenation. Catal Commun 89:77–80. https://doi.org/10.1016/j.catcom.2016.10.023

34. Tarabanko VE, Chernyak MYu, Simakova IL, Kaigorodov KL, Bezborodov YuN, Orlovskaya NF (2015) Antiknock properties of furfural derivatives. Russ J Appl Chem 88(11):1778–1782. https://doi.org/10.1134/S10704272150110063

35. Simakova IL, Tarabanko VE, Chernyak MY, Kondrasenko AA, Simonov MN (2015) Catalytic hydrogenation of furfural in alcoholic media. J Sib Fed Univ Chem 8(4):482–490. https://doi.org/10.17516/1998-2836-2015-8-4-482-490

36. Lange J-P, van der Ev Heide, van Buijtenen J, Price R (2012) Furfural—a promising platform for lignocellulosic biofuels. Chemsuschem 5(1):150–166. https://doi.org/10.1002/cssc.201100648

37. Sitthisa S, Resasco DE (2011) Hydrodeoxygenation of furfural over supported metal catalysts: a comparative study of Cu, Pd and Ni. Catal Lett 141(6):784–791. https://doi.org/10.1007/s10562-011-0581-7

38. Yan K, Wu G, Lafleur T, Jarvis C (2014) Production, properties and catalytic hydrogenation of furfural to fuel additives and value-added chemicals. Renew Sustain Energy Rev 38:663–676. https://doi.org/10.1016/j.rser.2014.07.003

39. Ponomarenko IV, Parfenov VA, Zaitseva YN, Kirik SD, Zharkov SM (2014) Template synthesis of CMK-3 nanostructured carbon material and study of its properties. Glass Phys Chem 40(10):79–87. https://doi.org/10.1134/S1087659614010180

40. Lashdaf M, Hatanpää T, Tiitta M (2001) Volatile β-diketonato complexes of ruthenium, palladium and platinum—preparation and thermal characterization. J Therm Anal Calorim 64(3):1171–1182. https://doi.org/10.1023/A:1011549130134

41. DeWolfe RH (1970) Carboxylic ortho acid derivatives: preparation and synthetic applications: preparation and synthetic applications. Academic Press Inc., New York, p 568p

42. Keegstra MA, Peters THA, Brandsma L (1992) Copper(I) halide catalysed synthesis of alkyl aryl and alkyl heteroaryl ethers. Tetrahedron 148(17):3633–3652. https://doi.org/10.1016/S0040-4020(01)88501-X

43. Rietveld HM (1969) A profile refinement method for nuclear and magnetic structures. J Appl Cryst 2(2):65–71. https://doi.org/10.1107/S0021889869006558

44. Solyanikova AS, Chayka MY, Boryak AV, Kravchenko TA, Glotov AV, Ponomarenko IV, Kirik SD (2014) Composite electrodes of electrochemical capacitors based on carbon materials with different structure. Russ J Electrochem 50(5):419–428. https://doi.org/10.1134/S1023193514050097

45. Isakova VG, Isakov VP, Lyamkin AI, Zharikova NV, Yunoshev AS, Nemtsev IV (2015) Surface modification of detonation nanodiamonds with platinum and palladium nanoparticles. Int J Chem 7(1):1–9. https://doi.org/10.5539/ijc.v7n1p1

46. Vargas Garcia JR, Goto T (2003) Deposition of iridium, platinum, rhodium and palladium. Mater Trans 44(9):1717–1728. https://doi.org/10.2320/matertrans.44.1717

47. Utriainen M, Kröger-Laukkanen M, Johansson L-S, Niinistö L (2000) Studies of metallic thin film growth in an atomic layer epitaxy reactor using M(acac)₂ (M = Ni, Cu, Pt) precursors. Appl Surf Sci 157(3):151–158. https://doi.org/10.1016/S0169-4332(99)00562-0

48. Ralph TR, Hogarth MP (2002) Catalysis for low temperature fuel cells. Part 1: the cathode challenges. Platin Met Rev 46(1):3–14

49. Belousov OV, Dorokhova LI, Solov'ev LA, Zharkov SM (2007) Change in the particle size of highly dispersed palladium black in hydrochloric acid solutions at elevated temperatures. Russ J Phys Chem A 81(8):1303–1306. https://doi.org/10.1134/s0036024407080237

50. Simakova IL, Solkina Y, Deliy I, Wärnå J, Murzin DY (2009) Modeling of kinetics and stereoselectivity in liquid-phase α-pinene hydrogenation over Pd/C. Appl Catal A 356(2):216–224. https://doi.org/10.1016/j.apcata.2009.01.006

51. Delidovich IV, Taran OP, Matvienko LG, Simonov AN, Simakova IL, Bobrovskaya AN, Parmon VN (2010) Selective oxidation of glucose over carbon-supported Pd and Pt catalysts. Catal Lett 140(1–2):14–21. https://doi.org/10.1007/s10562-010-0430-0

52. Ershov MA, Grigor'eva EV, Guseva AI, Vinogradova NYa, Potanin DA, Dorokhov VS, Nikul'shin PA, Ovchinnikov KA (2017) A review of furfural derivatives as promising octane boosters. Russ J Appl Chem 90(9):1402–1411. https://doi.org/10.1134/s1070427217090051

53. Reyes P, Salinas D, Campos C, Oportus M, Murcia J, Rojas H, Fierro JLG (2010) Selective hydrogenation of furfural on Ir/TiO₂ catalysts. Quim Nova 33(4):777–780. https://doi.org/10.1590/S0100-40422010000400002

54. Gulyaev RV, Kibis LS, Stonkus OA, Shubin YuV, Korenev SV, Ivanova AS, Slavinskaya EM, Zaikovskii VI, Danilova IG, Boronin AI, Sobyanin VA (2011) Synergetic effect in PdAu/CeO₂ catalysts for the low-temperature oxidation of CO. J Struct Chem 52(1):123–136. https://doi.org/10.1134/S002247661

55. Yu WY, Mullen GM, Flaherty DW, Mullins CB (2014) Selective hydrogen production from formic acid decomposition on Pd–Au bimetallic surfaces. J Am Chem Soc 136(31):11070–11078. https://doi.org/10.1021/ja505192v

56. Maeland AJ, Flanagan TB (1967) Comparison of hydrogen and deuterium solubility in palladium-rich alloys, gold–palladium. J Phys Chem 71(6):1950–1952. https://doi.org/10.1021/j100865a072

57. Koss U, Łukaszewski M, Hubkowska K, Czerwiński A (2011) Influence of rhodium additive on hydrogen electrosorption in palladium-rich Pd–Rh alloys. J Solid State Electrochem 15(11–12):2477–2487. https://doi.org/10.1007/s10008-011-1511-8